JACS
JOURNAL OF THE AMERICAN CHEMICAL SOCIETY
Communication
pubs.acs.org/JACS

Fabrication of an Efficient $BaTaO_2N$ Photoanode Harvesting a Wide Range of Visible Light for Water Splitting

Masanobu Higashi,[†] Kazunari Domen,[‡] and Ryu Abe*[,†,§]

[†]Graduate School of Engineering, Kyoto University, Katsura, Nishikyo-ku, Kyoto 615-8510, Japan
[‡]Department of Chemical System Engineering, The University of Tokyo, 7-3-1 Hongo, Tokyo 113-8565, Japan
[§]JSPS-NEXT Program, 5-3-1 Koujimachi, Chiyoda-ku, Tokyo 102-0083, Japan

Supporting Information

ABSTRACT: Photoanodes made from $BaTaO_2N$ that can harvest visible light up to 660 nm wavelength were fabricated on Ti substrates for achieving efficient water splitting. Both pre-treatment of $BaTaO_2N$ particles with an H_2 stream and post-necking treatment with $TaCl_5$ effectively increased the photocurrent due to the decreased electrical resistance in the porous $BaTaO_2N$ photoanode. A combination of pre-loading of CoO_x on the $BaTaO_2N$ particles and post-loading of RhO_x significantly improved both the photocurrent and stability under visible light irradiation, along with an obvious negative shift (ca. 300 mV) of the onset potential for water oxidation, while sole loading resulted in a lower photocurrent or insufficient stability. The IPCE value was estimated to be ca. 10% at 1.2 V vs RHE under 600 nm, which is the highest among photoanode materials that can harvest light beyond 600 nm for water oxidation. Photoelectrochemical water splitting into H_2 and O_2 under visible light was demonstrated using $RhO_x/CoO_x/BaTaO_2N$/Ti photoanodes under an externally applied bias larger than 0.7 V to a Pt counter electrode.

Photoelectrochemical (PEC) water splitting using semiconductor photoelectrodes has attracted considerable attention due to the potential to produce H_2 from water by utilizing solar energy, as well as to achieve photocatalytic water splitting using semiconductor particles.[1−4] Since nearly half of the solar energy incident on the Earth's surface lies in the visible region (400 nm < λ < 800 nm), it is essential to harness visible light, especially its long-wavelength region as long as possible, to realize efficient and practical H_2 production on a large scale by PEC water splitting. However, this is still hindered by the major challenge of developing photoelectrode materials that simultaneously have appropriate band energies, exhibit visible light absorption, and are sufficiently stable under reaction conditions. Since oxide semiconductors generally possess high stability against photocorrosion (photo-oxidative decomposition or dissolution), visible-light-responsive oxides (e.g., WO_3,[5] Fe_2O_3,[6] and $BiVO_4$[7]) have been extensively studied as photoanodes in PEC water splitting systems. However, it is indispensable to apply a large external bias between these oxide-based photoanodes and a counter electrode (e.g., Pt) because the bottoms of the conduction band of these visible-light-responsive oxides are more positive than the water reduction potential. Since applying a large external bias using a power supply is undesirable in terms of the energy consumption of the whole system, it is highly desirable to develop visible-light-driven PEC systems that can function even under much lower applied bias, simultaneously harvesting a wide range of visible light. It has been demonstrated that some metal oxynitrides (e.g., TaON,[8] $LaTiO_2N$[9]) possess appropriate band levels for water reduction and oxidation as well as a narrow bandgap, allowing visible light absorption due to the contribution of the N 2p orbital to the valence band with O 2p. Although the introduction of the N 2p orbital generates a new problem in stability due to oxidative deactivation by photogenerated holes releasing N_2 ($2N^{3-} + 6h^+ \rightarrow N_2$),[8] the above-mentioned features of oxynitrides make them promising semiconductor materials for achieving efficient PEC water splitting under visible light with low applied bias.

We recently demonstrated stable water splitting on a CoO_x-modified TaON porous photoanode, wherein the CoO_x nanoparticles as a catalyst for water oxidation[10−12] effectively scavenge the holes in TaON, suppressing oxidative deactivation of the TaON surface.[13] However, the maximum solar energy conversion efficiency of a TaON photoanode system is limited by the relatively wide band gap of TaON (ca. 2.5 eV, light absorption up to 500 nm). These facts motivated us to apply a mixed tantalum oxynitride $BaTaO_2N$ as a photoanode material, since it can harvest visible light up to 660 nm[14,15] and it possesses a sufficiently high conduction band bottom for H_2 production.[16] Although a photoanode of a solid solution of $BaZrO_3$−$BaTaO_2N$ fabricated on fluorine-doped tin oxide (FTO) exhibited the capability of water oxidation after loading of the IrO_x cocatalyst, it showed low IPCE values (e.g., 1%, at 1.2 V vs RHE under 500 nm) and required relatively large applied bias (1 V) between the Pt counter electrode to observe appreciable amounts of H_2 and O_2.[17] In the present study, we attempted to fabricate an efficient $BaTaO_2N$ photoanode for water splitting by applying two new strategies: (1) pre-treatment of $BaTaO_2N$ particles with an H_2 stream to decrease the electrical resistance, and (2) surface modification of the porous $BaTaO_2N$ electrode by the RhO_x species along with pre-loading of CoO_x to facilitate hole transfer from the $BaTaO_2N$ bulk.

$BaTaO_2N$ powder was prepared by heating an amorphous $Ba_2Ta_2O_7$ precursor powder in an NH_3 stream (100 mL min^{-1})

Received: April 23, 2013
Published: June 28, 2013

   dx.doi.org/10.1021/ja404030x | J. Am. Chem. Soc. 2013, 135, 10238−10241

at 1223 K for 20 h, as reported previously.[18] As shown in Figure S1, the main phase of the product were identified to $BaTaO_2N$ (ICDD No. 01-084-1748), while weak peaks assignable to the Ta_3N_5 phase were also observed. The obtained powder was heated in a H_2 flow at 1073 K for 3 h (referred to as $BaTaO_2N(H_2)$), washed with distilled water, and then dried at room temperature. CoO_x cocatalyst (0.5 or 3 wt%, calculated as a metal) was loaded on $BaTaO_2N(H_2)$ (or untreated $BaTaO_2N$) particles by impregnation from an aqueous $Co(NO_3)_2$ solution, followed by heating at 673 K for 30 min in air (referred to as $CoO_x/BaTaO_2N(H_2)$). As-prepared $CoO_x/BaTaO_2N(H_2)$ particles were deposited on a Ti substrate by electrophoretic deposition.[13] The representative amount and thickness of the $BaTaO_2N$ layer on Ti were ca. 2.6 mg and ca. 2 μm, respectively. The coated area was ca. 1.5 × 4 cm^2. Next, 50 μL of $TaCl_5$ methanol solution (10 mM) was dropped on the as-prepared electrodes, and then the electrode was dried in air at room temperature. After this process was performed five times, the electrode was heated in an NH_3 flow (10 mL min^{-1}) at 723 K for 30 min.[13] The resulting $CoO_x/BaTaO_2N(H_2)$ electrode was heated in a H_2 flow at 723 K for 30 min. These processes are referred to as the necking treatment. Post-loading of the MO_x cocatalyst on the $BaTaO_2N$ photoanode was performed as follows. $Co(NO_3)_2$, $Na_2[IrCl_6]$, or $Na_3[RhCl_6]$ methanol solution (Co, Ir, and Rh: 3 wt%) was dropped on the CoO_x(0.5 wt%)/$BaTaO_2N(H_2)$ electrode after the calcination in the NH_3 flow. The electrode was then dried and heated in a H_2 flow at 723 K for 30 min. $CoO_x/BaTaO_2N(H_2)$ and $BaTaO_2N(H_2)$ samples post-loaded with the cocatalyst were referred to as post-$MO_x/CoO_x/BaTaO_2N(H_2)$ and post-$MO_x/BaTaO_2N(H_2)$, respectively. The electrochemical cell used for the photocurrent measurements consisted of a prepared $BaTaO_2N$ electrode, a counter electrode (Pt wire), a Ag/AgCl reference electrode, and a phosphate buffer solution (pH 8). The phosphate buffer solution was prepared by mixing 0.1 M Na_2HPO_4(aq) and 0.1 M NaH_2PO_4(aq). The potential of the working electrode was controlled using a potentiostat. The solution was purged with Ar for over 20 min prior to the measurement. The electrodes were irradiated by a 300 W Xe lamp (LX-300F, Cermax) fitted with a cutoff filter (L-42, Hoya) to block light in the ultraviolet (UV) region. The detailed experimental conditions are given in Supporting Information.

Figure 1 shows the current−potential curves for the $BaTaO_2N$ electrodes in a phosphate buffer solution (pH 8) under chopped visible light irradiation (λ > 400 nm). Although no photoresponse was observed for the $BaTaO_2N$/Ti electrode just after electrophoretic deposition, the necking treatment, which effectively forms conductive necking between $BaTaO_2N$ particles, afforded an obvious photoresponse to visible light, as shown in Figure 1a, in the same manner as in the TaON/Ti and TaON/FTO electrode systems.[13,19,20] In the present $BaTaO_2N$/Ti electrode system, it was newly found that H_2 reduction of the $BaTaO_2N$ particles before their deposition on Ti significantly increased the photocurrent density, as shown in Figure 1b, in which approximately 4 times higher photocurrent density (ca. 0.46 mA cm^{-2} at 1.2 V vs RHE) was obtained compared to the untreated one (ca. 0.12 mA cm^{-2} at 1.2 V vs RHE). The optimum temperature of the H_2 treatment was found to be 1073 K, as shown in Figure S2. Figure S3 shows the UV−visible diffuse reflectance spectra of the $BaTaO_2N$ powder before and after the H_2 reduction at various temperatures. As-prepared $BaTaO_2N$ powder exhibited strong absorption shorter than 680 nm due to the bandgap excitation, along with broad absorption longer than

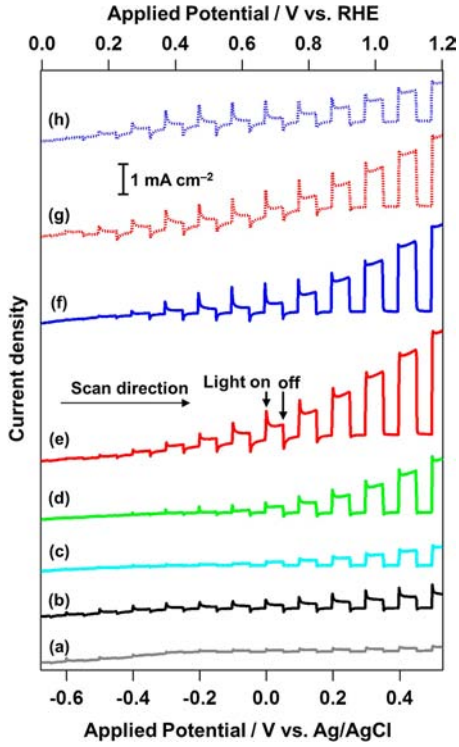

Figure 1. Current−potential curves in a phosphate buffer solution (pH 8) under visible light irradiation (λ > 400 nm) for (a) $BaTaO_2N$, (b) $BaTaO_2N(H_2)$, (c) CoO_x(3 wt%)/$BaTaO_2N$, (d) CoO_x(3 wt%)/$BaTaO_2N(H_2)$, (e) post-RhO_x(3 wt%)/CoO_x(0.5 wt%)/$BaTaO_2N(H_2)$, (f) post-IrO_x(3 wt%)/CoO_x(0.5 wt%)/$BaTaO_2N(H_2)$, (g) post-RhO_x(3 wt%)/$BaTaO_2N(H_2)$, and (h) post-IrO_x(3 wt%)/$BaTaO_2N(H_2)$ electrodes.

680 nm, which generally reflect the presence of reduced species of Ta^{5+} or anion defects, O^{2-} or N^{3-} vacancies, in the n-type semiconductors.

The H_2 treatment above 1073 K significantly increased the absorption intensity longer than 680 nm, indicating the increased amount of anion defects in the $BaTaO_2N$ particle. It is well recognized that the increased amount of anion defects in an n-type semiconductor increases the n-type nature; in other words, it decreases the electro resistance in the bulk. Indeed, impedance measurements revealed that the electro resistance in the $BaTaO_2N$ bulk was significantly decreased by the H_2 reduction treatment at 1073 K. It can therefore be concluded that the H_2 treatment decreased the electro resistance in the $BaTaO_2N$ bulk along with the necking process, and increased the photocurrent density in the $BaTaO_2N$/Ti electrodes consequently. The decrease in photocurrent density by the H_2 treatment above 1173 K is certainly due to superfluous anion defects, which work as electron-trapping sites and increase the possibility of electron−hole recombination within the $BaTaO_2N$ bulk. Similar to the TaON electrode system reported previously,[13] the loading of the CoO_x cocatalyst was found to be effective to improve the stability of the photoelectrode during the photoirradiation, as well as increasing photocurrent density. The CoO_x-loaded $BaTaO_2N$ electrodes (Figure 1c) showed appreciably higher photocurrent density than the unloaded one (Figure 1a). The optimum amount of CoO_x loaded on $BaTaO_2N$ was found to be 3 wt% Co, as shown in Figure S4. The combination of CoO_x loading with H_2 treatment was effective to increase the photocurrent density (Figure 1d), undoubtedly due to the

dx.doi.org/10.1021/ja404030x | J. Am. Chem. Soc. 2013, 135, 10238−10241

decreased electro resistance in the $BaTaO_2N$ bulk. Although the loading of CoO_x significantly increased the photocurrent density at applied potentials higher than 0.6 V (vs RHE), on the contrary this decreased the photocurrents at potentials lower than 0.6 V, which were clearly observed for the unloaded $BaTaO_2N(H_2)$ (Figure 1b). We found that post-loading of RhO_x (or IrO_x) with the pre-loaded CoO_x was effective to increase the photocurrent densities at the whole potential range above 0.2 V (vs RHE), as shown in Figure 1e,f. The post-RhO_x (or IrO_x)/CoO_x/$BaTaO_2N$ electrode showed an obvious negative shift (ca. 300 mV) of the onset potential. Post-loading of RhO_x (or IrO_x) alone was found to be effective to improve the photocurrent densities at lower applied potential (0.2−0.6 V vs RHE, see Figure 1g,h), while their co-loadings with pre-loaded CoO_x additionally increased the photocurrent at higher potential than 0.6 V.

The loading of co-catalysts significantly affected the stability of the photocurrent generated on $BaTaO_2N$ electrodes. As seen in the time courses of the photocurrent under potentiostatic condition (1.07 V vs RHE, see Figure 2), the photocurrent over

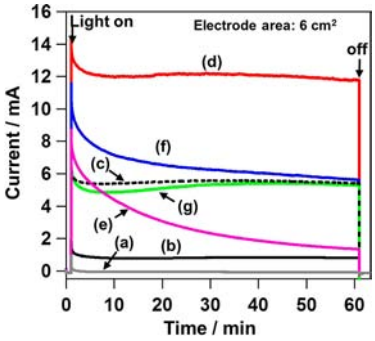

Figure 2. Time courses of photocurrent at 1.07 V (vs RHE) in a phosphate buffer solution (pH 8) under visible light irradiation for (a) $BaTaO_2N(H_2)$, (b) CoO_x(0.5 wt%)/$BaTaO_2N(H_2)$, (c) CoO_x(3.0 wt %)/$BaTaO_2N(H_2)$, (d) post-RhO_x(3 wt%)/CoO_x(0.5 wt %)/$BaTaO_2N(H_2)$, (e) post-RhO_x(3 wt%)/$BaTaO_2N(H_2)$, (f) post-IrO_x(3 wt%)/CoO_x(0.5 wt%)/$BaTaO_2N(H_2)$, and (g) post-CoO_x(3 wt %)/CoO_x(0.5 wt%)/$BaTaO_2N(H_2)$ electrodes.

the unloaded $BaTaO_2N(H_2)$ electrode immediately decreased and became negligibly low within 5 min (Figure 2a), undoubtedly due to the deactivation of the $BaTaO_2N$ surface during the photoirradiation, in which holes generated in the $BaTaO_2N$ bulk oxidize the nitrogen anion (N^{3-}) to N_2 ($2N^{3-} + 6h^+ \rightarrow N_2$) just the same as in the previous TaON electrode system.[13,19,20] The loading of CoO_x (0.5 or 3 wt%) on $BaTaO_2N$ particles prior to the electrode fabrication drastically improved the stability of the photocurrent as seen in Figure 2b,c, indicating that the CoO_x loaded on $BaTaO_2N$ efficiently scavenged the holes generated in the $BaTaO_2N$ bulk and also efficiently catalyzed water oxidation, suppressing the self-oxidative deactivation of the surface by the holes.[13] Among the CoO_x(0.5 wt%)/$BaTaO_2N(H_2)$ electrodes post-loaded with various cocatalysts, the RhO_x (3 wt%)-loaded one exhibited the highest photocurrent as well as surpassingly high stability (see Figure 2d). On the other hand, the $BaTaO_2N(H_2)$ electrode post-loaded with RhO_x alone showed poor stability (see Figure 2e), while the photocurrent in the initial period was much higher than that on the unmodified $BaTaO_2N(H_2)$ or CoO_x/$BaTaO_2N(H_2)$ electrodes. XPS analysis on RhO_x/CoO_x/$BaTaO_2N(H_2)$ electrode (see Figure S5) indicated that it dominantly contained metallic Rh species along with minor components of oxidized ones just after the H_2 treatment, while most of them were oxidized into Rh^{3+} species, most likely Rh_2O_3, after the PEC measurement. Although the post-loading of IrO_x significantly increased the photocurrent in the initial period, the photocurrent gradually decreased, as seen in Figure 2f. The post-CoO_x(3 wt%)/CoO_x(0.5 wt%)/$BaTaO_2N(H_2)$ electrode (Figure 2g) showed almost the same trend as the CoO_x(3 wt %)/$BaTaO_2N(H_2)$ electrode (Figure 2c). These results suggested that the combination of pre-loaded CoO_x with post-loaded RhO_x exhibits a kind of synergistic effect for achieving efficient and stable water oxidation on the $BaTaO_2N$ photoanode. Although the catalytic ability of the CoO_x species for water oxidation has been proven in extensive studies,[21−23] that of RhO_x has not yet been clarified. Thus, one possible explanation for the synergistic effect observed would be that the RhO_x species acted as a facilitator of hole transfer between the $BaTaO_2N$ surface and CoO_x, whereas water oxidation dominantly proceeded on the CoO_x. For example, the loaded Rh^{3+} species captured the holes generated in the $BaTaO_2N$ bulk, yielding highly oxidized species such as Rh^{4+}, which then transfer the holes to the dispersed CoO_x particles (0.5 wt%). The highly dispersed RhO_x containing Rh^{3+} species might efficiently capture holes from the $BaTaO_2N$, improving the efficiency in charge separation (e^- and h^+), especially under a low applied potential, resulting in a significant increase in photocurrent densities as an applied potential lower than 0.6 V (vs RHE) as seen in Figure 1e,g. Figure S6 shows the STEM image of particles peeled from the post-RhO_x(3 wt%)/CoO_x(0.5 wt%)/$BaTaO_2N(H_2)$ electrode, along with the results on elemental mappings of Co and Rh. Fine particles with diameters of 2−5 nm were highly dispersed on the whole surface of $BaTaO_2N$, while it was difficult for us to distinguish RhO_x from CoO_x. However, the elemental mappings indicate that both the Co and Rh species are homogeneously dispersed, except for the partially observed segregations. These results will support the speculated effect of co-loading of CoO_x and RhO_x, in which charge transfer efficiency occurs between them. Of course, one cannot exclude the possibility that the RhO_x species work as a cocatalyst facilitating water oxidation, along with CoO_x. However, $BaTaO_2N$ loaded with RhO_x alone showed rather poor stability (see Figure 2e). This strongly suggested that the catalytic activity of RhO_x was insufficient for complete consumption of holes, inducing backward hole transfer from RhO_x to $BaTaO_2N$, which caused oxidative deactivation of the $BaTaO_2N$ surface. Pre-loaded RhO_x/$BaTaO_2N$ particles could not be deposited by the electrophoretic method. The detailed reaction mechanism is under investigation.

Figure 3 shows the IPCE action spectra of the $BaTaO_2N$ photoanodes in a phosphate buffer solution (pH 8). The post-loading of RhO_x on CoO_x/$BaTaO_2N$ afforded a clear increase in IPCE values at lower potential (0.6−0.8 V vs RHE). The improvement in IPCE was observed not only in the phosphate buffer solution but also in Na_2SO_4(aq), as shown in Figure S7. These results again indicated the significant effect of combining pre-loaded CoO_x with post-loaded RhO_x on improving the efficiency in charge separation in the low applied potential regions. Although the thresholds of the IPCE spectra were in good agreement with that of the absorption of $BaTaO_2N$ (at around 680 nm), the shapes were slightly different from the absorption. The impurity Ta_3N_5 (absorption edge: 600 nm) component in $BaTaO_2N$ particles or TaON-like phase formed by a necking treatment[20] might contribute to the photocurrent. The obtained IPCE value (e.g., 10% at 1.2 V vs RHE at 600 nm) of the

dx.doi.org/10.1021/ja404030x | J. Am. Chem. Soc. 2013, 135, 10238−10241

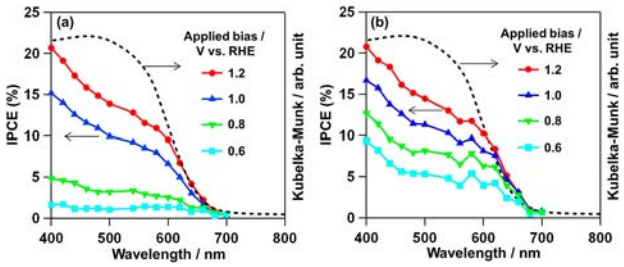

Figure 3. IPCE spectra of (a) CoO_x(3 wt%)/$BaTaO_2N(H_2)$ and (b) post-RhO_x(3 wt%)/CoO_x(0.5 wt%)/$BaTaO_2N(H_2)$ electrodes with various applied potentials (phosphate buffer solution, pH 8), and absorption spectrum of $BaTaO_2N$.

$RhO_x/CoO_x/BaTaO_2N(H_2)$ photoanode was the highest among photoanode materials with band gap smaller than 2.0 eV (corresponding to light absorption at 600 nm), which can oxidize water as shown below.

Figure 4 shows the time course of H_2 and O_2 evolution over the $RhO_x/CoO_x/BaTaO_2N(H_2)$ photoanode under visible light

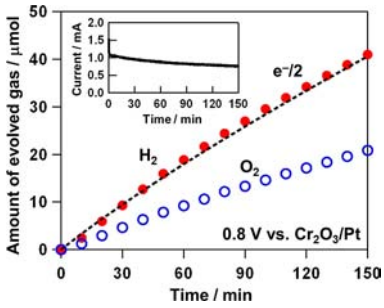

Figure 4. Time course of gas evolution in a two-electrode system composed of post-RhO_x(3 wt%)/CoO_x(0.5 wt%)/$BaTaO_2N(H_2)$ electrode and Pt-wire coated with Cr_2O_3 in a phosphate buffer solution (pH 8) under visible light irradiation. The inset indicates the change in the photocurrent.

irradiation with an applied bias of 0.8 V vs counter electrode. A Pt wire coated with Cr_2O_3 was employed as a counter electrode due to suppression of water formation from H_2 and O_2, that is, an undesirable backward reaction, on the Pt surface.[24] H_2 and O_2 evolved close to the stoichiometric ratio. The amounts of gases evolved in 150 min (H_2, 41.0 μmol; O_2, 20.9 μmol) exceeded the molar amounts of $BaTaO_2N$ (ca. 7.1 μmol), CoO_x cocatalyst (ca. 1.0 μmol, calculated as CoO), and RhO_x (ca. 0.75 μmol, calculated as Rh) in the electrode. The amount of H_2 evolved was in agreement with half of the electrons passing through the outer circuit ($e^-/2$, indicated by the broken line), indicating that the obtained photocurrent was derived from water splitting. As shown in Figure S8, it was confirmed that PEC water splitting using the $RhO_x/CoO_x/BaTaO_2N(H_2)$ photoanode proceeded at more than 0.7 V vs counter electrode.

Efficient $BaTaO_2N$ photoanodes that can harvest a wide range of visible light for water splitting were thus successfully fabricated on Ti substrates through a combination of electrophoretic deposition and post-necking methods. Both the treatment of $BaTaO_2N$ particles by H_2 and co-loading of CoO_x and RhO_x cocatalysts significantly increased the photocurrent efficiency, as well as caused a negative shift in the onset potential for water splitting. PEC water splitting under visible light was thus demonstrated using the $RhO_x/CoO_x/BaTaO_2N(H_2)$ photoanode under an externally applied bias of 0.7 V (vs Pt).

■ ASSOCIATED CONTENT

Supporting Information

UV−visible diffuse reflectance spectra and XRD pattern of $BaTaO_2N$ powder, IPCE spectra of $BaTaO_2N$ electrode, STEM image, and PEC water splitting result. This material is available free of charge via the Internet at http://pubs.acs.org.

■ AUTHOR INFORMATION

Corresponding Author

ryu-abe@scl.kyoto-u.ac.jp

Notes

The authors declare no competing financial interest.

■ ACKNOWLEDGMENTS

This work was supported by JSPS-NEXT Program, JST-CREST Program, and Nanotechnology Platform Program of MEXT.

■ REFERENCES

(1) Maeda, K.; Domen, K. *J. Phys. Chem. C* **2007**, *111*, 7851−7861.
(2) Kudo, A.; Miseki, Y. *Chem. Soc. Rev.* **2009**, *38*, 253−278.
(3) Esswein, M. J.; Nocera, D. G. *Chem. Rev.* **2007**, *107*, 4022−4047.
(4) Abe, R. *J. Photochem. Photobiol. C* **2010**, *11*, 179−209.
(5) Santato, C.; Ulmann, M.; Augustynski, J. *J. Phys. Chem. B* **2001**, *105*, 936−940.
(6) Kay, A.; Cesar, I.; Gratzel, M. *J. Am. Chem. Soc.* **2006**, *128*, 15714−15721.
(7) Sayama, K.; Nomura, A.; Arai, T.; Sugita, T.; Abe, R.; Yanagida, M.; Oi, T.; Iwasaki, Y.; Abe, Y.; Sugihara, H. *J. Phys. Chem. B* **2006**, *110*, 11352−11360.
(8) Hitoki, G.; Takata, T.; Kondo, J. N.; Hara, M.; Kobayashi, H.; Domen, K. *Chem. Commun.* **2002**, 1698−1699.
(9) Kasahara, A.; Nukumizu, K.; Hitoki, G.; Takata, T.; Kondo, J. N.; Hara, M.; Kobayashi, H.; Domen, K. *J. Phys. Chem. A* **2002**, *106*, 6750−6753.
(10) Jiao, F.; Frei, H. *Angew. Chem., Int. Ed.* **2009**, *48*, 1841−1844.
(11) Kanan, M. W.; Nocera, D. G. *Science* **2008**, *321*, 1072−1075.
(12) Brimblecombe, R.; Koo, A.; Dismukes, G. C.; Swiegers, G. F.; Spiccia, L. *J. Am. Chem. Soc.* **2010**, *132*, 2892−2894.
(13) Higashi, M.; Domen, K.; Abe, R. *J. Am. Chem. Soc.* **2012**, *134*, 6968−6971.
(14) Pors, F.; Marchand, R.; Laurent, Y.; Bacher, P.; Roult, G. *Mater. Res. Bull.* **1988**, *23*, 1447−1450.
(15) Kim, Y. I.; Woodward, P. M.; Baba-Kishi, K. Z.; Tai, C. W. *Chem. Mater.* **2004**, *16*, 1267−1276.
(16) Hitoki, G.; Takata, T.; Kondo, J. N.; Hara, M.; Kobayashi, H.; Domen, K. *Electrochemistry* **2002**, *70*, 463−465.
(17) Maeda, K.; Domen, K. *Angew. Chem., Int. Ed.* **2012**, *51*, 9865−9869.
(18) Higashi, M.; Abe, R.; Teramura, K.; Takata, T.; Ohtani, B.; Domen, K. *Chem. Phys. Lett.* **2008**, *452*, 120−123.
(19) Abe, R.; Higashi, M.; Domen, K. *J. Am. Chem. Soc.* **2010**, *132*, 11828−11829.
(20) Higashi, M.; Abe, R.; Domen, K. *Energy Environ. Sci.* **2011**, *4*, 4138−4147.
(21) Gerken, J. B.; McAlpin, J. G.; Chen, J. Y. C.; Rigsby, M. L.; Casey, W. H.; Britt, R. D.; Stahl, S. S. *J. Am. Chem. Soc.* **2011**, *133*, 14431−14442.
(22) Stracke, J. J.; Finke, R. G. *J. Am. Chem. Soc.* **2011**, *133*, 14872−14875.
(23) Barroso, M.; Cowan, A. J.; Pendlebury, S. R.; Gratzel, M.; Klug, D. R.; Durrant, J. R. *J. Am. Chem. Soc.* **2011**, *133*, 14868−14871.
(24) Yoshida, M.; Takanabe, K.; Maeda, K.; Ishikawa, A.; Kubota, J.; Sakata, Y.; Ikezawa, Y.; Domen, K. *J. Phys. Chem. C* **2009**, *113*, 10151−10157.